Carbon 121 (2017) 322–329

Contents lists available at ScienceDirect

Carbon

journal homepage: www.elsevier.com/locate/carbon

Carbon structure in nanodiamonds elucidated from Raman spectroscopy

Vitaly I. Korepanov [a], Hiro-o Hamaguchi [a, *], Eiji Osawa [b], Vladimir Ermolenkov [c], Igor K. Lednev [c], Bastian J.M. Etzold [d], Olga Levinson [e], Boris Zousman [e], Chandra Prakash Epperla [f], Huan-Cheng Chang [f]

[a] National Chiao-Tung University, Taiwan
[b] NanoCarbon Research Ltd., Japan
[c] Department of Chemistry, University at Albany, SUNY, USA
[d] Technische Universität Darmstadt, Ernst-Berl-Institut für Technische und Makromolekulare Chemie, Alarich-Weiss-Straße 8, 64287, Darmstadt, Germany
[e] Ray Techniques Ltd, Jerusalem, 91391, Israel
[f] Institute of Atomic and Molecular Sciences, Academia Sinica, Taiwan

ARTICLE INFO

Article history:
Received 1 March 2017
Received in revised form
2 June 2017
Accepted 3 June 2017
Available online 3 June 2017

Keywords:
Nanocarbon
Raman spectroscopy
Nanoparticles
Structure
Phonon confinement
Particle size

ABSTRACT

Despite their name, nanodiamonds (ND) are comprised of a complex interplay of different carbon phases. The diamond core is surrounded by the shell consisting mostly of disordered sp^3 carbon and graphene-like carbon (GLC). The complex structure makes the characterization of nanodiamonds (ND) a difficult challenge. Recent development of many varieties of NDs for different applications demands quick and reliable characterization of the content of various carbon fragments, as well as the estimation of the diamond core size. In this work, we apply Raman spectroscopy to study the structure of nanodiamonds from different origins, including those produced by detonation (DND), high pressure high temperature synthesis (HPHT), and pulsed laser irradiation (LND). The relative content of GLC, disordered and surface carbon can be easily determined from Raman spectra. In particular, we show how the content of different structure fragments is changed upon de-agglutination, surface oxidation and ion irradiation. We also compare the different ND production methods in terms of the structural uniformity of the nanoparticles. Raman spectroscopy provides unique quantitative tool for ND characterization; we believe that the present data will be useful for understanding the structure of diamond nanoparticles, and will provide the background for obtaining the NDs with desired properties.

1. Introduction

Diamonds nanoparticles represent a unique class of nanoscale systems with variable structure and tunable properties. At present, they can be obtained by several synthetic routes with different grain size ranging from sub-5 nm detonation nanodiamond (DND) to 10–1000 nm high-pressure-high-temperature (HPHT) nanodiamonds. Despite the commonly used term “nanodiamonds”, these nanoparticles comprise a complex interplay of different carbon phases. The structure can be perceived as more or less crystalline diamond core surrounded by the shell, consisting of graphene-like carbon (GLC), disordered sp3 carbon and surface-state carbon [1–4]. The latter includes *trans*-polyacetylene (TPA) chains [5,6] GLC islets and fullerene-like fragments [7]. Besides carbon structure fragments, a number of functional groups is found on the surface, including C–H and oxygen-containing groups (=-OH, >C=O), the relative amount of which depends on the chemical history of the sample [8–10]. Some portion of the amorphous sp3 and GLS shell can be eliminated, for example, by oxidation or plasma etching [11,12]. However, GLC islets, fullerene-like fragments and TPA are intrinsic components of the shell, coming from the re-arrangement of the diamond surface [7]. With the decrease of the particle size, the shell plays increasingly important role in physical and chemical properties of the material.

The wide range of the particle sizes, and easily achievable variety of surface terminations result in numerous applications of

* Corresponding author. Department of Applied Chemistry, Institute of Molecular Science, National Chiao Tung University, 1001 Ta-Hsueh Road, Hsinchu, 30010, Taiwan.
E-mail address: hhama@nctu.edu.tw (H.-o. Hamaguchi).

http://dx.doi.org/10.1016/j.carbon.2017.06.012
0008-6223/

NDs in biomedicine, material technology, abrasives, lubricants, imaging, and many other fields [2]. The fast and reliable characterization of different carbon phases and their changes upon different physical and chemical treatments is of major importance for the ND-related research and technology. The structure of diamond nanoparticles has been studied previously by many methods, including TEM [1,4], XPS [13–15], and others [10,13–17]. Numerous Raman studies have also been performed, mostly for detonation nanodiamonds. It was shown that Raman spectroscopy is sensitive to the particle size [18,19], can probe the surface functional groups [8] and gives the information on different carbon phases [6,9,20].

In the present work, we attempt a systematic study of the carbon phases content in NDs by Raman spectroscopy. We consider the ND samples of different synthetic origin, commonly used in research and industry, including detonation (DND), high pressure high temperature synthesis (HPHT), and pulsed laser irradiation (LND). We propose a quantification procedure, which allows one to derive the crystallite size information from the Raman pattern, and to analyze how the content of the carbon structural fragments is influenced by the common techniques of ND processing, including de-agglutination, surface oxidation and nitrogen ion irradiation.

1.1. Raman spectra and assignment of the bands

The complexity of ND structure is revealed in the Raman spectra as a superposition of bands coming from the nanocarbon fragments of different bonding [6,20]. The Raman cross-sections for different nanocarbon types also depend on the excitation wavelength in different ways [6]. On the other side, the bands coming from different structure fragments can be easily identified and distinguished, which makes it possible to characterize the relative content of those in the material.

The assignment of the spectral features of different nanocarbons is by now well established; the reader can refer to the works [6,8,20] and references therein for more details. We summarize the spectral assignment in Fig. 1, with the spectra measured at three different excitation wavelengths for the same sample.

The major bands in the Raman spectra of NDs are:

1) The diamond band for the bulk crystal is observed as a sharp line at around 1333 cm^{-1}; for ND it gives a broad peak in 1290–1350 cm^{-1} region, the position and width depends on the crystallite size.
2) Graphene-like carbon gives the G and D peaks, which lie at ~1560 and 1360 cm^{-1} respectively [6]. The G peak position shows dispersion (excitation wavelength dependence) [6]. In our experiments, the D peak is most pronounced at 200 nm excitation, while in the 355 and 532 nm spectra it appears as a shoulder. The G band is partially superimposed with the 1640 cm^{-1} band of water [8].
3) Disordered sp3 carbon gives a broad feature in 1100–1350 cm^{-1}, the shape of which corresponds to the density of states (DOS) [20].
4) *Trans*-poly-acetylene carbon on the surface gives a peak at around 1150 cm^{-1} [20,21].
5) The dumbbell, or split-interstitial defect of the diamond lattice, shows a relatively sharp band at 1630 cm^{-1} [20].

In the present work, we aimed to study the structure of nanodiamonds of different origins, and examine the impact of various treatment procedures on the structure. As can be seen from Fig. 1, most convenient for this purpose is to use the distinct bands of diamond, disordered sp^3 carbon and G-band of GLC measured at 355 nm excitation, because the contribution from non-carbon bands is relatively low, and the bands from different carbon fragments can be easily distinguished from each other.

It is worth mentioning that there is no general "Raman spectrum of ND", because the spectral pattern strongly depends on the content of different carbon phases. For instance, the spectrum of the raw detonation soot under 325 nm excitation is dominated by GLC bands to an extent that no diamond peak is observed, and only after oxidation of sp^2 phase the 1327 cm^{-1} peak becomes pronounced [8].

1.2. Experimental detection of the ND Raman spectra

The main difficulty of the experimental detection of ND Raman spectra is that the sample is typically the black powder, which absorbs the light throughout the whole UV–Vis spectral range. Therefore, under the laser beam the sample can be easily heated or burned out. To overcome this problem, different groups either use low laser power or try to measure under water [22]. From our experience, the use of rotating cell with the ND sample dispersed in water allows one to obtain high signal-to-noise ratio spectra without the need to reduce the laser power [23]. In addition to that, this technique helps to avoid the thermal distortion of the phonon spectrum, and provides a good averaging over the sample.

Another challenge is to achieve good signal-to-noise ratio. Most of ND samples give quite strong luminescence, coming, most likely, from GLC fragments on the surface. The luminescence dominates the spectrum at 632.8 nm excitation to an extent that practically no Raman band is observable for most of the samples. With decreasing excitation wavelength the Raman-to-luminescence ratio becomes higher. Under deep UV (200 nm) practically no luminescence is observed. On the other hand, in deep UV spectra many Raman bands from surface groups and defects become quite strong (see Fig. 1) which makes it difficult to analyze the carbon bands. From our results, the reasonable balance is to use UV excitation at 355 nm, under which the luminescence background can be easily subtracted, and the Raman bands of different carbon fragments can be distinguished.

From our observation, the Raman-to-luminescence ratio can also be significantly improved by the oxidation of the surface carbon (e.g. 425 °C in air), therefore for some measurements the samples can be pre-treated to get better spectra.

1.3. "Raman size" of nanodiamonds

The crystallite size estimation is of major importance for the numerous applications of nanodiamond. The common techniques used for that purpose include transmission electron microscopy (TEM), dynamic light scattering (DLS), X-ray diffraction and small-angle X-ray diffraction (SAXS). It must be understood that these methods by their nature are supposed to estimate different physical parameters. TEM can give the image of the particles at the focal plane, and, therefore, give a rough estimate of the particle size and the crystallite size for a very limited portion of the sample. The DLS measures hydrodynamic radius, which includes surface layers and detects aggregates as a single particle. X-ray diffraction used with the Scherrer equation possesses certain degree of arbitrariness, although for high signal-to-noise ratio diffraction patterns the size distribution of crystallites still can be roughly estimated [24]. The disadvantage of XRD is the low sensitivity to the size. The SAXS is a reliable and sensitive method for estimating the grain size of nanopowders [25]. The grain size although does not coincide with the diamond core size, because SAXS does not make distinction between different types of carbon.

The "Raman size" for crystalline materials can be defined as the phonon confinement length, or, in other words, the size of coherently scattering domain. In case of diamond it corresponds to the

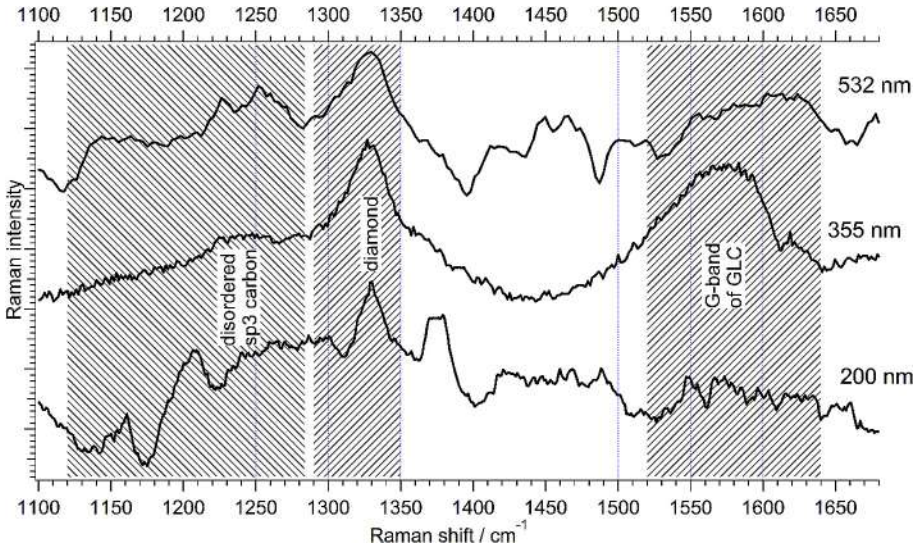

Fig. 1. Experimental Raman spectra of 3 nm DND at different excitation wavelengths; the major bands of different carbon phases highlighted.

crystallite size of the diamond core, because Raman spectroscopy can distinguish the diamond lattice band from the other structural fragments. Other advantages of Raman spectroscopy are relatively high size sensitivity, statistical reliability and comparatively simple experimental measurement.

The established approach linking the Raman band shape to the phonon confinement length, known as Phonon Confinement Model (PCM) was proposed by Richter [26]. Applying it to carbon nanoparticles, many research groups used simplified one-dimensional description of the phonon dispersion [18,22,27–30]. For materials with pronounced anisotropy of the phonon dispersion, however, such approach introduces certain degree of arbitrariness. Diamond is a well known example of such system [31].

We have recently reported the physically consistent way of building the PCM, which includes not only 3D phonon dispersion, but also size distribution and other minor improvements. Hereafter, we will use the working formula from the work [23]:

$$I(\omega) \cong \int \rho(\sigma) d\sigma \frac{\sigma^3}{N(\sigma)} \iiint \frac{\Gamma_0(\sigma) * |C(q_0, q)|^2}{(\omega - \omega(q))^2 + (\Gamma_0(\sigma)/2)^2} d^3q \qquad (1)$$

where ω is the wavenumber, $\rho(\sigma)$ is the particle size distribution, $N(\sigma)$ is the normalizing factor, $\Gamma_0(\sigma)$ is the natural bandwidth, $C(q_0,q)$ is the Fourier coefficient, and $\omega(q)$ is the three-dimensional (3D) phonon dispersion function. As has been shown before [23], the good description of the dispersion function can be obtained using scaled quantum-chemical frequencies. The PCM has proved to adequately account for the size dependence of the Raman spectra of nanodiamonds. The simulated spectral patterns of monodisperse NDs of different size are shown in Fig. 2.

2. Materials and methods

2.1. ND samples and procedures of physical and chemical treatment

We have used the following ND samples for the present study.

- DND3, de-agglutinated detonation nanodiamond colloid, with mean size of 3.3 nm (as estimated from DLS), NanoCarbon Research Institute Ltd., Japan.
- DND3 irradiated with nitrogen ions. Experimental set-up was provided as a courtesy of Nagata Seiki, Japan. 20 keV nitrogen beam was used. The nitrogen pressure at the plasma generator was $3.5*10^{-2}$ Pa; the current was 20 μA. The sample load was 300 mg. Irradiation was performed 2 times during 40 min. In between the two irradiations the sample was carefully mixed.
- DND3 agglutinates, the raw material used for the production of DND3.
- DND3 oxidized, the DND3 sample after oxidation in air at 420 °C within 20hr.
- DND LbL0, the ND from Adamas Nanotechnologies Inc.
- DND LbL15, the DND LbL0 sample after 15 cycles of Layer-by-Layer oxidation [25].
- LND, laser-synthesized ND with 4 nm mean size (as estimated by XRD), Ray Techniques Ltd., Israel;
- 23 nm HPHT, high-pressure high-temperature diamond from Microdiamant AG, acid-washed and air-oxidized (3–4 h at 450 °C), with mean size 23 nm (as estimated by DLS), Institute of Atomic and Molecular Sciences, Academia Sinica, Taiwan.
- 29 HPHT diamond, treated in the same way, with mean size 29 nm (as estimated by DLS),
- 42 HPHT diamond, treated in the same way, with mean size 42 nm (as estimated by DLS).

2.2. Spectral measurements

The spectra under 200 nm excitation were measured with a lab-built spectroscopic system in quasi-backscattering geometry at Albany [32]; the laser power was 2 mW, the signal was accumulated for 30 min. The 355 nm measurements were done with a lab-built set-up at Hsinchu. The de-focused laser beam was used (~1 mm in diameter, ~60 mW); the signal was collected at 90°. The accumulations time was 30 min. The measurements under 532 nm excitation were made with a lab-built set-up at Hsinchu in confocal geometry at laser power 12 mW with 30 min accumulation time. The 632.8 nm measurements were made with a confocal lab-built set-up at Hsinchu with 2–20 mW laser power with accumulation time 10 min.

For measurements under 200 nm, 355 nm and 532 nm the samples were in the form of the 1 wt% ND colloid in water. The colloids were ultrasonicated in a horn during at least 0.5 h prior to

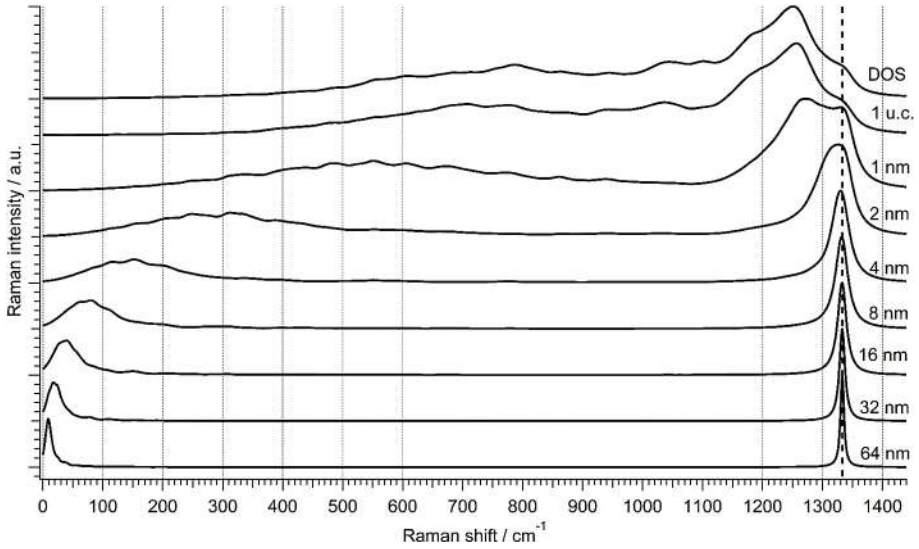

Fig. 2. Calculated Raman spectra for different confinement lengths starting with disordered sp3 carbon network (DOS), next is 1 unit cell (1 u.c.) confinement (i.e. 0.3567 nm). The dashed line indicates the frequency at the Γ point (1332.9 cm^{-1}).

the measurement. To avoid the effects of laser heating, which may significantly distort the spectrum [33], the rotating quartz cell was used.

2.3. Computational procedures

The PCM fitting of the diamond band was performed as described in our previous paper [23]. The 3D phonon dispersion of diamond $\omega(q)$ was calculated with Quantum Espresso software [34] and scaled uniformly to match the experimental zone-center energy. This $\omega(q)$ was used directly for the numerical integration over q (eq. (1)). As was shown before, the sufficient integration limit is 2.0 in terms of the reduced wave-vector coordinate [23].

For the calculation of the Fourier coefficients, the 3D step-function was used. Such approach has been used for a long time in crystallography for the description of diffraction pattern from nanocrystalline powders [23]. It has been shown that for spherical nanoparticles the Fourier coefficients take form of the Bessel function:

$$C(q_0, q) = \frac{4}{3}\pi R^3 \left[3\frac{\sin(qR) - qR*\cos(qR)}{(qR)^3}\right] \quad (2)$$

The fit of the experimental Raman spectra with the phonon confinement model was made with the Matlab (2014b) script. Since the first order diamond line (around 1332.9 cm^{-1}) is superimposed by the disordered sp3 carbon line (broad feature at 1240 cm^{-1}) and D-band of graphene-like carbon (1368 cm^{-1}), the fit was made only for the 1270-1355 cm^{-1} region, where the first order diamond line is the most distinct. The particle size distribution $\rho(\sigma)$ was assumed to be Normal with small contribution of log-Normal to describe the fact that nanodiamonds typically contain a few percent of relatively large particles [35].

3. Results and discussions

3.1. Size dependence and quantification procedure

The Raman spectra of the major ND samples with different sizes are shown on Fig. 3. For the bulk diamond the spectrum has only one sharp symmetric line, while for NDs the shape of the diamond band displays the pronounced size dependence. Its asymmetrical broadening is a result of the phonon confinement (discussed above, see Fig. 2). Besides that, in nanodiamond samples GLC band and amorphous sp3 bands become prominent (~1200 and 1580 cm^{-1}). Since the corresponding structural fragments are located on the surface of the nanoparticles, their intensity follows general trend of surface-to-volume ratio (i.e. for smaller particles the intensity is higher). The bands above 1650 cm^{-1} most likely, belong to the carbonyl groups on the surface, or to isolated C=C bonds.

Since the spectra were measured in water colloid under constant rotation, no laser heating effect is expected in the spectra. According to the test measurement with ND concentration in the range 0.05–5 wt%, there is no significant contribution of water to the spectral pattern. The highest signal-to-noise ratio was achieved at 1% concentration, which was chosen as a standard for most measurements.

In the present work, the diamond line was fitted with the PCM (eq. (1)) to estimate the crystallite size. After that, the diamond peak was subtracted and the ratios (area intensities) of the diamond line, G-band of GLC and the amorphous diamond band were estimated. This procedure is illustrated in Fig. 4. The results are summarized in Table 1.

The PCM reproduces the size dependence of the diamond band quite well, in both asymmetry and band width. The “Raman size” obtained from fitting with eq. (1) shows a good agreement with the size estimated by other methods, including DLS, TEM and XRD [23]. The results allow us to estimate the upper limit of the PCM applicability, which is about 50 nm. Above this value, both experimental and simulated spectra become close to those of the bulk crystal (Figs. 2 and 3). Note that the spacial dimensions of the phonon confinement are is significantly larger than the range of quantum electron confinement effect, which is 1.57 nm [36].

It should be noted that in the present work we use the PCM in the approximation of the spherical particles. This description holds quite well for small particles of DND and LND [17]. For relatively big HPHT ND, the particles have “uniform and blocky” shape according to the manufacturer (Microdiamant AG). The ND samples studied here are commonly used in research, and for all of them the TEM images are available in the literature: for DND [1,4], LND [37–40] and HPHT ND [41–43]. Based on these images, it is reasonable to assume spherical shapes for them.

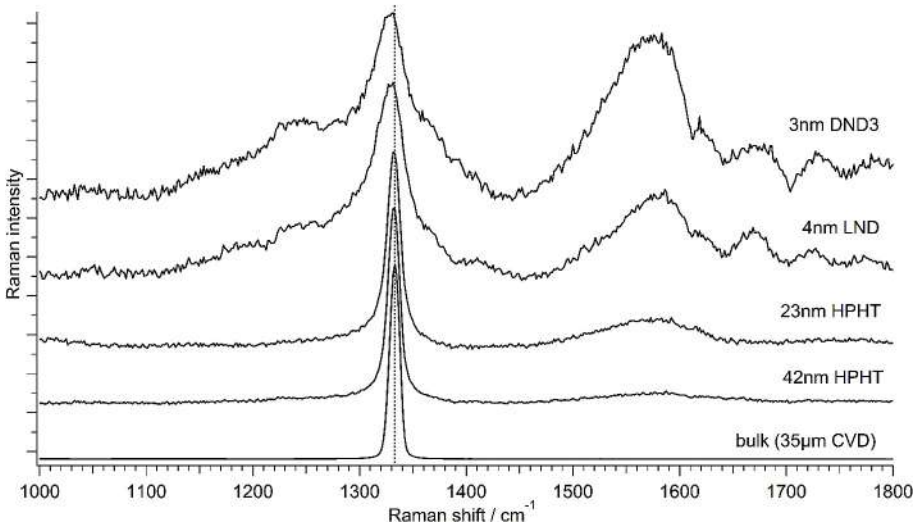

Fig. 3. Representative Raman spectra of ND samples of different mean size and origin under 355 nm excitation. Size in this figure is given as estimated by DLS for HPHT and DND3 samples and by XRD for the LND one. The position of the zone-center phonon (1332.9 cm^{-1}) is indicated by the dotted line.

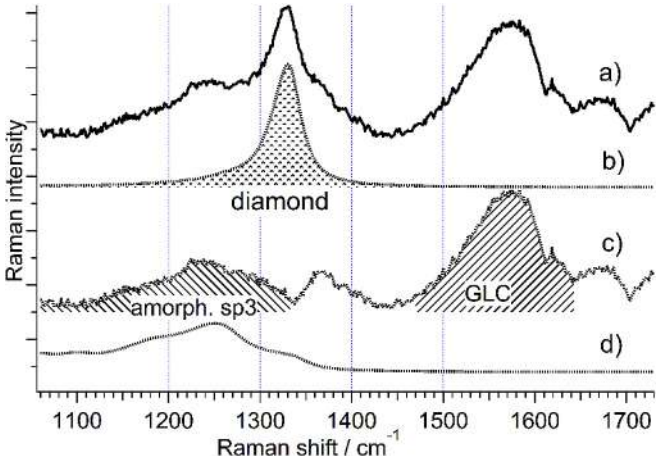

Fig. 4. The procedure of analyzing the ND spectra: the experimental spectrum (a), fit of the diamond band with PCM equation (b), ND spectrum after subtraction of the diamond band (c), DOS of diamond shown to confirm assignment of the amorphous diamond band (d). (A colour version of this figure can be viewed online.)

Strictly speaking, for non-spherical particles the Fourier coefficients should be different from the Bessel-like functions used here. In principle, one can numerically calculate $C(q_0,q)$ for any arbitrary particle shape [44], but to include in the model both size distribution and shape distribution directly would be quite cumbersome. However, in the present case, because the pronounced crystallographic orientation of the crystallites is absent, the shape distribution is equivalent to the spreading over the confinement lengths, therefore the size distribution $\rho(\sigma)$ effectively account for the shape variations also. This makes the proposed approach physically sound.

This quantification procedure allows us to compare the different ND production method, as well as to analyze how the structure of ND particles is influenced by the common techniques of ND processing, such as de-agglutination, surface oxidation and ion irradiation.

3.2. The effect of de-agglutination

The process of preparation of well-dispersed ND colloid, also known as de-agglutination, includes beads milling and ultrasonication [45]. During the beads milling, the local pressure and temperature can be high enough to have impact on the nanoparticle structure. By means of Raman spectroscopy we can study what was the change.

As can be seen from Table 1, the diamond-to-amorphous carbon ratio is increased slightly upon de-agglutination, while the diamond-to-GLC ratio is decreased. The difference in the spectra between raw and de-agglutinated samples is shown in Fig. 5. Thus, the local pressure and temperature induce moderate graphitization, most likely graphitized might be the amorphous sp3 carbon from the ND shell. The crystallite size of the ND doesn't show

Table 1
Quantitative analysis of the Raman spectra of different nanodiamond samples.

Sample[a]	Median size estimated from PCM, nm	Median size by other methods, nm	Diamond to amorphous ratio	Diamond to GLC ratio
De-agglutinated DND (DND3)	2.9	3.3 (DLS)	1.02	0.55
DND3 irradiated with N_2^+	2.2	–	0.71	0.32
DND3 oxidized in air	2.9	2.7 (DLS)	1.41	1.17
raw DND3 agglutinates	2.9	–	0.89	0.82
DND LbL 0	3.0	5.2 (SAXS)	0.88	0.86
DND LbL 15	3.0	4.8 (SAXS)	1.42	1.05
laser-synthesized ND (LND)	3.5	4.0 (XRD)	1.27	1.12
23 nm HPHT ND (ox)	21.6	23 (DLS)	2.30	1.24
29 nm HPHT ND (ox)	28.8	29 (DLS)	3.16	2.52
42 nm HPHT ND (ox)	42.4	42 (DLS)	2.51	2.46

[a] See materials and methods section for more details about the history of the samples.

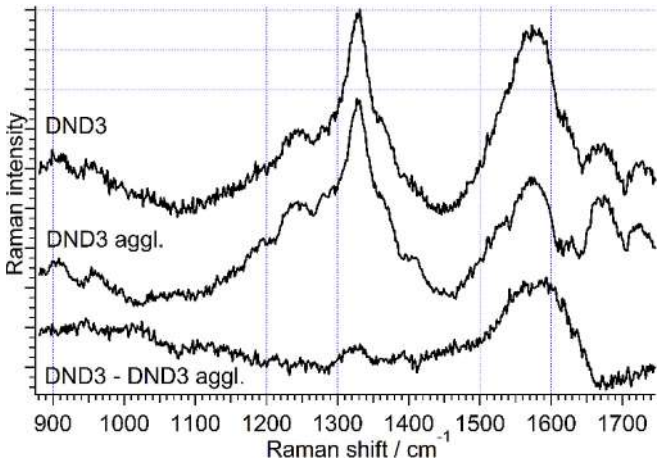

Fig. 5. Raman spectra under 355 nm excitation of de-agglutinated DND3 (top), initial agglutinates (middle) and the difference (bottom).

detectable difference which indicates that the diamond core remains practically the same.

3.3. The effect of surface oxidation

The controlled oxidation of nanodiamonds is expected to reduce the particle size. On the other hand, since smaller particles are expected to burn out more quickly, the average particle size may also increase. It is also reasonable to expect that defective carbon would oxidize more easily than highly ordered. We studied by Raman spectroscopy the ND samples after two different modes of oxidation: by air and layer-by-layer (LbL). In contrast to air oxidation, the LbL etching allows one to avoid a runaway oxidation reaction of small particles [25]. The oxidation in air was performed at relatively soft temperature of 425 °C during 20 h (mean DLS size reduced from 3.3 to 2.7 nm); the LbL etching was done within 15 sorption-desorption cycles (the SAXS size reduced from 5.2 to 4.8 nm).

The spectra of oxidized NDs are compared to those of starting samples in Fig. 6. It can be seen that in both oxidation regimes the difference spectrum has major contribution from D and G peaks of GLC along with amorphous carbon bands. The peaks on the both sides of diamond band (1270-1370 cm^{-1}) can also belong to very small crystallites (below 1 nm), see Fig. 2.

The surprising finding is that the raw and oxidized spectra have almost identical diamond band, which is hardly distinguishable by PCM. From the point of view of ND structure it means that the surface is covered by GLC and amorphous carbon, which is etched in both oxidation modes, while the diamond core remains practically unchanged. This indicates that the particle size decrease detected by SAXS in LbL etching and DLS in air oxidation can be assigned mostly to the etching of non-diamond carbon from the nanoparticle shell.

3.4. The effect of nitrogen ion irradiation

Ion irradiation, typically used to introduce defects in diamond lattice, has quite strong impact on the ND structure. As can be seen from Table 1 and Fig. 7, the G-band of GLC (~1600 cm^{-1}) becomes almost twice stronger after the irradiation, the pronounced increase of amorphous sp3 carbon band is also observed. These results corroborate the previous computational studies [46].

The diamond crystallite size determination by PCM is less reliable in case of irradiated sample, because the diamond peak is strongly superimposed by other bands. However, the PCM results in this case show quite expected decrease of phonon confinement length, which can be attributed most likely to the confinement by the lattice defects.

3.5. Comparison of ND production methods

The main quantitative criteria to compare the production methods of NDs are the peak ratios of diamond to GLC and diamond to amorphous sp^3 carbon. From Table 1 it can be seen that the raw DND agglutinates both from NCRI (DND3) and Adamas Nanotechnologies (DND LbL 0) have lower content of diamond than LND. The raw HPHT diamonds have very high GLC content, which didn't allow us to measure the Raman spectra of un-oxidized samples. For the oxidized ones, the diamond content is relatively high, but taking into account the much higher particle size, the GLC content is still very significant. Therefore, among the studied samples, the most structurally uniform diamond nanoparticles seem to be produced by the laser irradiation. The structural uniformity of NDs can be significantly improved by the surface oxidation.

4. Conclusions

Raman spectra provide key information on the structure of nanodiamonds, such as relative content of different carbon phases and the crystallite size. This allows us to study the behavior of different structure fragments during chemical and physical treatment. Diamond nanoparticles consist of the inert and stable diamond core, surrounded by the shell of amorphous sp3 carbon and GLC, which more easily undergoes transformations. Thus, deagglutination procedure is accompanied by minor graphitization of the shell due to local heat/pressure effect. Oxidation treatment in both layer-by-layer and air-oxidation regimes results in the

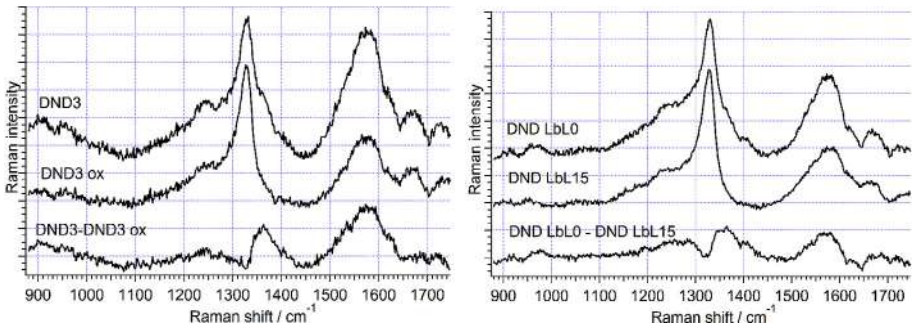

Fig. 6. Oxidation of ND by air (left) and layer-by-layer etching (right). Top curves: spectra of original samples, middle: oxidized, bottom: difference. The Raman spectra were measured under 355 nm excitation. (A colour version of this figure can be viewed online.)

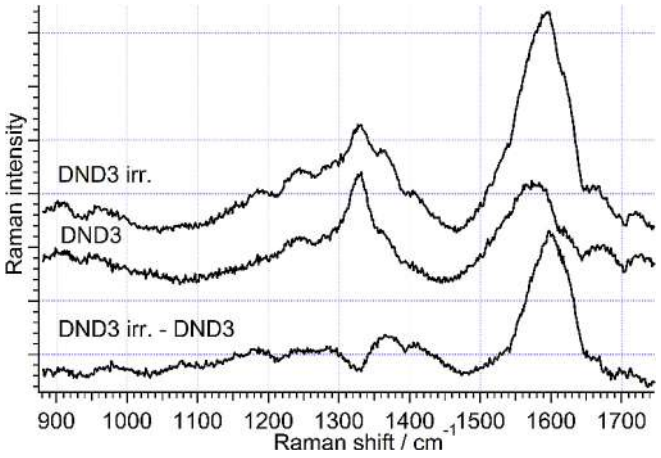

Fig. 7. The effect of nitrogen ions irradiation on the ND structure: Raman spectra under 355 nm excitation of irradiated sample (top), original sample (middle), and the difference (bottom).

decrease of GLC and amorphous carbon content, while the diamond core remains practically the same. The irradiation of NDs with nitrogen ions results in both decrease of the crystallite size and pronounced graphitization.

Quantitative study of the Raman spectra of different NDs makes it possible to compare different ND production methods in terms of the structural uniformity of the resulting material. Among the studied samples (DND, LND, HPHT-ND) the laser-assisted synthesis gives the most pure "diamond" material with lowest content of GLC and amorphous carbon. The structural uniformity of NDs can be significantly improved by the surface oxidation under mild conditions.

Raman spectroscopy is an important quantitative tool to analyze the ND spectra. We believe the present results would assist the synthesis of the NDs with desired properties and boost the development of the nanocarbon technology.

Acknowledgements

The authors acknowledge Prof. Yury Gogotsi (Drexel University) for the nanodiamond samples (DND LbL). The work was supported by the Ministry of Science and Technology of Taiwan (MOST105-2113-M-009-002 and MOST105-2745-M-009-001-ASP) and the Ministry of Education of Taiwan ("Aim for the Top University Plan" of National Chiao Tung University).

References

[1] K. Iakoubovskii, K. Mitsuishi, K. Furuya, High-resolution electron microscopy of detonation nanodiamond, Nanotechnology 19 (2008) 155705, http://dx.doi.org/10.1088/0957-4484/19/15/155705.
[2] V.N. Mochalin, O. Shenderova, D. Ho, Y. Gogotsi, The properties and applications of nanodiamonds, Nat. Nanotechnol. 7 (2011) 11–23, http://dx.doi.org/10.1038/nnano.2011.209.
[3] E. Osawa, Single-nano buckydiamond particles. Synthesis strategies, characterization methodologies and emerging applications, in: D. Ho (Ed.), Nanodiamonds Appl. Biol. Nanoscale Med, Springer US, 2010, pp. 1–33, http://dx.doi.org/10.1007/978-1-4419-0531-4_1.
[4] O. Shenderova, A. Koscheev, N. Zaripov, I. Petrov, Y. Skryabin, P. Detkov, S. Turner, G. Van Tendeloo, Surface chemistry and properties of ozone-purified detonation nanodiamonds, J. Phys. Chem. C 115 (2011) 9827–9837, http://dx.doi.org/10.1021/jp1102466.
[5] K.V. Reich, Optical properties of nanodiamond suspensions, JETP Lett. 94 (2011) 22–26, http://dx.doi.org/10.1134/S0021364011130169.
[6] A.C. Ferrari, J. Robertson, Raman spectroscopy of amorphous, nanostructured, diamond-like carbon, and nanodiamond, Philos. Trans. A. Math. Phys. Eng. Sci. 362 (2004) 2477–2512, http://dx.doi.org/10.1098/rsta.2004.1452.
[7] Y.V. Novakovskaya, A.V. Vorontsov, Typical surface segments of diamond-core carbon nanoparticles, Struct. Chem. 26 (2015) 1297–1307, http://dx.doi.org/10.1007/s11224-015-0644-2.
[8] V. Mochalin, S. Osswald, Y. Gogotsi, Contribution of functional groups to the raman spectrum of nanodiamond powders, Chem. Mater 21 (2009) 273–279, http://dx.doi.org/10.1021/cm802057q.
[9] M. Mermoux, A. Crisci, T. Petit, H.A. Girard, J.-C. Arnault, Surface modifications of detonation nanodiamonds probed by multiwavelength raman spectroscopy, J. Phys. Chem. C 118 (2014) 23415–23425, http://dx.doi.org/10.1021/jp507377z.
[10] G.C.C. Costa, O. Shenderova, V. Mochalin, Y. Gogotsi, A. Navrotsky, Thermochemistry of nanodiamond terminated by oxygen containing functional groups, Carbon N. Y. 80 (2014) 544–550, http://dx.doi.org/10.1016/j.carbon.2014.08.094.
[11] R. Martín, M. Alvaro, J.R. Herance, H. García, Fenton-treated functionalized diamond nanoparticles as gene delivery system, ACS Nano 4 (2010) 65–74, http://dx.doi.org/10.1021/nn901616c.
[12] S. Osswald, G. Yushin, V. Mochalin, S.O. Kucheyev, Y. Gogotsi, Control of sp2/sp3 carbon ratio and surface chemistry of nanodiamond powders by selective oxidation in air, J. Am. Chem. Soc. 128 (2006) 11635–11642, http://dx.doi.org/10.1021/ja063303n.
[13] H.A. Girard, T. Petit, S. Perruchas, T. Gacoin, C. Gesset, J.C. Arnault, P. Bergonzo, Surface properties of hydrogenated nanodiamonds: a chemical investigation, Phys. Chem. Chem. Phys. 13 (2011) 11517–11523, http://dx.doi.org/10.1039/c1cp20424f.
[14] J.-C. Arnault, T. Petit, H. Girard, A. Chavanne, C. Gesset, M. Sennour, M. Chaigneau, Surface chemical modifications and surface reactivity of nanodiamonds hydrogenated by CVD plasma, Phys. Chem. Chem. Phys. 13 (2011) 11481–11487, http://dx.doi.org/10.1039/c1cp20109c.
[15] O. Shenderova, A.M. Panich, S. Moseenkov, S.C. Hens, V. Kuznetsov, H.-M. Vieth, Hydroxylated detonation nanodiamond: FTIR, XPS, and NMR studies, J. Phys. Chem. C 115 (2011) 19005–19011, http://dx.doi.org/10.1021/jp205389m.
[16] J.A. Cuenca, E. Thomas, S. Mandal, O. Williams, A. Porch, Microwave determination of sp2 carbon fraction in nanodiamond powders, Carbon N. Y. 81 (2015) 174–178, http://dx.doi.org/10.1016/j.carbon.2014.09.046.
[17] A.S. Barnard, M. Sternberg, Crystallinity and surface electrostatics of diamond nanocrystals, J. Mater. Chem. 17 (2007) 4811, http://dx.doi.org/10.1039/b710189a.
[18] M. Yoshikawa, Y. Mori, H. Obata, M. Maegawa, G. Katagiri, H. Ishida, A. Ishitani, Raman scattering from nanometer-sized diamond, Appl. Phys. Lett. 67 (1995) 694, http://dx.doi.org/10.1063/1.115206.
[19] K.W. Sun, C.Y. Wang, Optical properties of a single free standing nanodiamond, J. Phys. Conf. Ser. 92 (2007) 12031, http://dx.doi.org/10.1088/1742-6596/92/1/012031.
[20] S. Prawer, K.W. Nugent, D.N. Jamieson, J.O. Orwa, L.A. Bursill, J.L. Peng, The Raman spectrum of nanocrystalline diamond, Chem. Phys. Lett. 332 (2000) 93–97, http://dx.doi.org/10.1016/S0009-2614(00)01236-7.
[21] A.C. Ferrari, J. Robertson, Origin of the 1150 cm^{-1} Raman mode in nanocrystalline diamond, Phys. Rev. B 63 (2001) 121405, http://dx.doi.org/10.1103/PhysRevB.63.121405.
[22] S. Osswald, V. Mochalin, M. Havel, G. Yushin, Y. Gogotsi, Phonon confinement effects in the Raman spectrum of nanodiamond, Phys. Rev. B 80 (2009) 75419, http://dx.doi.org/10.1103/PhysRevB.80.075419.
[23] V.I. Korepanov, H. Hamaguchi, Quantum-chemical perspective of nanoscale Raman spectroscopy with the three-dimensional phonon confinement model, J. Raman Spectrosc. (2017), http://dx.doi.org/10.1002/jrs.5132.
[24] R. Pielaszek, FW1/5/4/5M method for determination of the grain size distribution from powder diffraction line profile, J. Alloys Compd. 382 (2004) 128–132, http://dx.doi.org/10.1016/j.jallcom.2004.05.040.
[25] B.J.M. Etzold, I. Neitzel, M. Kett, F. Strobl, V.N. Mochalin, Y. Gogotsi, Layer-by-Layer oxidation for decreasing the size of detonation nanodiamond, Chem. Mater. 26 (2014) 3479–3484, http://dx.doi.org/10.1021/cm500937r.
[26] H. Richter, Z.P. Wang, L. Ley, The one phonon Raman spectrum in microcrystalline silicon, Solid State Commun. 39 (1981) 625–629, http://dx.doi.org/10.1016/0038-1098(81)90337-9.
[27] K.W. Sun, J.Y. Wang, T.Y. Ko, Raman spectroscopy of single nanodiamond: phonon-confinement effects, Appl. Phys. Lett. 92 (2008) 153115, http://dx.doi.org/10.1063/1.2912029.
[28] J. Ager, D. Veirs, G. Rosenblatt, Spatially resolved Raman studies of diamond films grown by chemical vapor deposition, Phys. Rev. B 43 (1991) 6491–6499, http://dx.doi.org/10.1103/PhysRevB.43.6491.
[29] A.K. Arora, T. Ravindran, G.L. Reddy, A.K. Sikder, D. Misra, Nature of confinement of phonons in nanocrystalline CVD diamond, Diam. Relat. Mater. 10 (2001) 1477–1485, http://dx.doi.org/10.1016/S0925-9635(00)00616-6.
[30] G. Katumba, B.W. Mwakikunga, T.R. Mothibinyane, FTIR and raman spectroscopy of carbon nanoparticles in SiO2, ZnO and NiO matrices, Nanoscale Res. Lett. 3 (2008) 421–426, http://dx.doi.org/10.1007/s11671-008-9172-y.
[31] J. Kulda, H. Kainzmaier, D. Strauch, B. Dorner, M. Lorenzen, M. Krisch, Overbending of the longitudinal optical phonon branch in diamond as evidenced by inelastic neutron and x-ray scattering, Phys. Rev. B 66 (2002) 241202, http://dx.doi.org/10.1103/PhysRevB.66.241202.
[32] I.K. Lednev, V.V. Ermolenkov, W. He, M. Xu, Deep-UV Raman spectrometer tunable between 193 and 205 nm for structural characterization of proteins, Anal. Bioanal. Chem. 381 (2005) 431–437, http://dx.doi.org/10.1007/s00216-004-2991-5.

[33] M. Chaigneau, G. Picardi, H.A. Girard, J.-C. Arnault, R. Ossikovski, Laser heating versus phonon confinement effect in the Raman spectra of diamond nanoparticles, J. Nanoparticle Res. 14 (2012) 955, http://dx.doi.org/10.1007/s11051-012-0955-9.

[34] P. Giannozzi, S. Baroni, N. Bonini, M. Calandra, R. Car, C. Cavazzoni, D. Ceresoli, G.L. Chiarotti, M. Cococcioni, I. Dabo, A. Dal Corso, S. de Gironcoli, S. Fabris, G. Fratesi, R. Gebauer, U. Gerstmann, C. Gougoussis, A. Kokalj, M. Lazzeri, L. Martin-Samos, N. Marzari, F. Mauri, R. Mazzarello, S. Paolini, A. Pasquarello, L. Paulatto, C. Sbraccia, S. Scandolo, G. Sclauzero, A.P. Seitsonen, A. Smogunov, P. Umari, R.M. Wentzcovitch, Quantum espresso: a modular and open-source software project for quantum simulations of materials, J. Phys. Condens. Matter 21 (2009) 395502, http://dx.doi.org/10.1088/0953-8984/21/39/395502.

[35] S. Stehlik, M. Varga, M. Ledinsky, V. Jirasek, A. Artemenko, H. Kozak, L. Ondic, V. Skakalova, G. Argentero, T. Pennycook, J.C. Meyer, A. Fejfar, A. Kromka, B. Rezek, Size and purity control of HPHT nanodiamonds down to 1 nm, J. Phys. Chem. C (2015), http://dx.doi.org/10.1021/acs.jpcc.5b05259, 150825003821009.

[36] H. Okushi, H. Watanabe, S. Yamasaki, S. Kanno, Emission properties from dense exciton gases in diamond, Phys. Status Solidi 203 (2006) 3226–3244, http://dx.doi.org/10.1002/pssa.200671410.

[37] B. Zousman, O. Levinson, Pure nanodiamonds produced by laser-assisted technique, in: O. Williams (Ed.), Nanodiamond, Royal Society of Chemistry, 2014, pp. 112–127.

[38] S. Hu, F. Tian, P. Bai, S. Cao, J. Sun, J. Yang, Synthesis and luminescence of nanodiamonds from carbon black, Mater. Sci. Eng. B 157 (2009) 11–14, http://dx.doi.org/10.1016/j.mseb.2008.12.001.

[39] J. Sun, S.-L. Hu, X.-W. Du, Y.-W. Lei, L. Jiang, Ultrafine diamond synthesized by long-pulse-width laser, Appl. Phys. Lett. 89 (2006) 183115, http://dx.doi.org/10.1063/1.2385210.

[40] D. Tan, S. Zhou, B. Xu, P. Chen, Y. Shimotsuma, K. Miura, J. Qiu, Simple synthesis of ultra-small nanodiamonds with tunable size and photoluminescence, Carbon N. Y. 62 (2013) 374–381, http://dx.doi.org/10.1016/j.carbon.2013.06.019.

[41] A. Wolcott, T. Schiros, M.E. Trusheim, E.H. Chen, D. Nordlund, R.E. Diaz, O. Gaathon, D. Englund, J.S. Owen, Surface structure of aerobically oxidized diamond nanocrystals, J. Phys. Chem. C 118 (2014) 26695–26702, http://dx.doi.org/10.1021/jp506992c.

[42] O. Beffort, S. Vaucher, F.A. Khalid, On the thermal and chemical stability of diamond during processing of Al/diamond composites by liquid metal infiltration (squeeze casting), Diam. Relat. Mater 13 (2004) 1834–1843, http://dx.doi.org/10.1016/j.diamond.2004.04.014.

[43] F.A. Khalid, O. Beffort, U.E. Klotz, B.A. Keller, P. Gasser, Microstructure and interfacial characteristics of aluminium–diamond composite materials, Diam. Relat. Mater. 13 (2004) 393–400, http://dx.doi.org/10.1016/j.diamond.2003.11.095.

[44] K. Roodenko, I. Goldthorpe, P. McIntyre, Y. Chabal, Modified phonon confinement model for Raman spectroscopy of nanostructured materials, Phys. Rev. B 82 (2010) 115210, http://dx.doi.org/10.1103/PhysRevB.82.115210.

[45] M. Ozawa, M. Inaguma, M. Takahashi, F. Kataoka, A. Krüger, E. Ōsawa, Preparation and behavior of brownish, clear nanodiamond colloids, Adv. Mater. 19 (2007) 1201–1206, http://dx.doi.org/10.1002/adma.200601452.

[46] F. Valencia, J.D. Mella, R.I. González, M. Kiwi, E.M. Bringa, Confinement effects in irradiation of nanocrystalline diamond, Carbon N. Y. 93 (2015) 458–464, http://dx.doi.org/10.1016/j.carbon.2015.05.067.